A Numerical Model to Predict Damaged Bearing Vibrations

SADOK SASSI
Department of Physics and Instrumentation, Institut National des Sciences Appliquées et de Technologie, Centre Urbain Nord, B.P. 676, 1080 Tunis Cedex, Tunisia

BECHIR BADRI
MARC THOMAS
Department of Mechanical Engineering, École de technologie supérieure, 1100, Notre-Dame Street West, Montreal, Quebec, (H3C 1K3), CANADA (marc.thomas@etsmtl.ca)

(Received 20 July 2006; accepted 31 January 2007)

Abstract: This work aims to develop the theoretical fundamentals and numerical details of new software, dedicated to the simulation of the dynamic behavior of rotating ball bearings in the presence of localized surface defects. In this article, the generation of vibration by a point defect in a rolling element bearing is modeled as a function of the rotation of the bearing, of the distribution of the load in the bearing, of the bearing structure elasticity, of the oil film characteristics, and of the transfer path between the bearing and the transducer. The numerical model is developed with the assumption that the dynamic behavior of the bearing can be represented by a coupled three-degree-of-freedom system, after which the governing equations of the simulation model are solved using computer simulation techniques. A new application, called BEAT (BEAring Toolbox), was developed in order to simulate bearings' vibratory response to the excitations produced by localized defects. By adding a noisy response due to the sliding friction occurring between the moving parts to the impulsive response caused by localized defects, the BEAT software is able to provide realistic results, similar to those produced by a sensor during experimental measurements.

Keywords: Vibration, bearing, defect, diagnostic

1. INTRODUCTION

Over recent decades, much progress has been achieved in the development of manufacturing processes, control techniques and maintenance. However, maintenance tools for manufacturing industries still require constant improvement. In a predictive machinery maintenance process, bearings being the most exposed parts are consequently more subject to degradation.

The role of a roller bearing inside a machine is to provide a high precision positioning and load-carrying capacity between a rotating shaft and a fixed housing, while maintaining low friction-torque, low vibration and low noise emission. It is simple in form and concept, but extremely effective in reducing friction and wear in a wide range of machinery products.

Journal of Vibration and Control, **13(11):** 1603–1628, 2007 DOI: 10.1177/1077546307080040

Figures 1, 2, 4–12 appear in color online: http://jvc.sagepub.com

Unfortunately, rolling bearings are subject to wear and accidents during their operation, and much still remains unknown about factors that could affect the longevity of bearings.

Despite the long history of the use of bearings and the vast experience that has been accumulated with regard to their load-carrying capacity and fatigue-life predictions, relatively few models have been proposed to explain the dynamic behavior of bearings subjected to localized or distributed defects. Investigations of bearing dynamics and their influence on an adjoining system were first conducted many decades ago, when the bearing was represented by a simple one- or two-degree-of-freedom (2 DoF) model, with linear springs, and with or without damping. In the early 1980s, a model was developed to describe the vibration produced by a single-point defect on the inner race of a rolling element bearing under constant radial load (McFadden and Smith, 1984). This model incorporated the effects of bearing geometry, shaft speed, bearing load distribution, transfer function and the exponential decay of vibration. A comparison between the predicted and measured demodulated vibration spectra confirms the relatively satisfactory performance of this model.

At about the same time, research performed by Sunnersjo (1985), explained in detail how surface irregularities are related to the vibration characteristics of the bearing. This study was restricted to radial bearings which had positive clearances and were subjected to radial loads. The approximate methods used produced results that were useful mainly for lightly loaded bearings operating at low and moderate speeds, with attention focused particularly on the effects of inner ring waviness and on the non-uniform diameters of the rolling elements. A mixed theoretical and experimental impedance approach was used to treat the bearing when fitted in a simple machine structure. The results showed how bearing vibrations can be calculated in terms of bearing/rotor parameters and foundation properties. Two common modes of surface deterioration (spalling fatigue and abrasive wear) were studied, with the practical objective being to highlight some possible methods of condition monitoring and prediction of impending bearing failure.

In the early 1990s, more refined bearing models were introduced, with the most significant improvement appearing in the 5 DoF bearing model from Lim and Singh (1990), which assumed rigid outer and inner rings and deformable balls. A mathematical model was subsequently proposed to illustrate the frequency characteristics of roller bearing vibrations due to surface irregularities arising from manufacturing errors (Su et al., 1993). The bearing vibration was modeled as the system output when it is subjected to excitations from surface waviness and roughness through the lubrication film. It was shown that the vibration spectrum of a normal bearing under a preloaded condition has a pattern of equal frequency spacing distribution that is similar to that of a defective bearing. Consequently, the application of frequency analysis on bearing monitoring, such as the high frequency resonance technique, should be undertaken with great care.

In the late 1990s, an analytical model was proposed for predicting the vibration frequencies of rolling bearings, as well as the amplitudes of significant frequency components caused by a localized defect on the outer race, the inner race or one of the rolling elements, under radial and axial loads (Tandon and Choudhury, 1997). This model predicted a discrete spectrum with peaks at the characteristic defect frequencies and harmonics. In the case of an inner race defect or a rolling element defect under a radial load, there are sidebands around each peak. The effect of load and pulse shape on the vibration amplitude was considered in the model. Typical numerical results for a ball bearing were obtained and plotted. A comparison with experimental values obtained from published literature showed that the model

could be successfully used to predict amplitude ratios among various spectral lines. Some authors investigated bearing-support models, with more detailed models used for adjoining systems (supports, spindles, etc.); in some cases however, less detailed bearing models were used (Shamine et al., 2000). Other researchers simply studied bearing-induced vibration without transmission phenomena (Spiewak and Nickel, 2001).

The analyses mentioned above were all linear; non-linear analyses used in investigating bearing dynamics are usually more complex with respect to both the bearing-support model definition and the transmission studies (El Saeidy, 1998).

For studying shaft-bearing-support systems, recent studies apply discretization principles, which are mainly approaches involving distributed parameter systems (Aleyaasin et al., 2000) and finite-element-based analyses in conjunction with various reduction and coupling methods (Fang and Yang, 1998), in the numerical and experimental senses. These methods deal with multiple degree-of-freedom (MDOF) systems, regardless of the type of analytical–numerical approach used.

The apparent simplicity of the physical system studied (the bearing contains only four mobile elements) can be misleading. In fact, many factors complicate the theoretically developed models. Often, the models cannot fully and satisfactorily explain the dynamic behavior of the bearing and the manner in which the induced vibration is influenced by bearing parameters.

This research therefore aims to provide a numerical simulation based on theoretical developments of the vibration response of a ball bearing affected by a localized defect. The generation of vibration by a point defect in a rolling element bearing is modeled as a function of the rotation of the bearing, the distribution of the load in the bearing, the transfer function between the bearing and the transducer, the elasticity of the bearing structure, and the elasto-hydro-dynamic oil film characteristics.

2. CHARACTERISTICS OF A BALL BEARING

2.1. Bearing Structure

A rolling-element bearing is an assembly of several parts: An inner race, an outer race, a set of balls or rollers, and a cage or a separator, which maintains even spacing for the rolling elements. The important geometrical parameters of the bearing are the number of rolling elements N_b, the ball diameter B_d, the average (pitch) diameter P_d and the contact angle α.

To analyze the structural vibrations affecting rolling element bearings, a number of assumptions are made here. The temperature of the entire bearing is assumed to be invariant with time. Only small elastic motions are considered, with all deformations governed by the Hertz theory of elasticity. The outer and inner bearing races are considered to be perfectly circular and rigidly fixed to the support and shaft (respectively), and all balls are presumed to be perfectly spherical and of equal diameter.

The calculation of the total vibration response of such a system is complicated by the non-linear behaviour of the bearing. A quasi-static method has been used, in which the bearing is considered a displacement generator, with just two rollers always carrying the load. This simple and approximate method gives satisfactory results for moderate speed lightly loaded bearings.

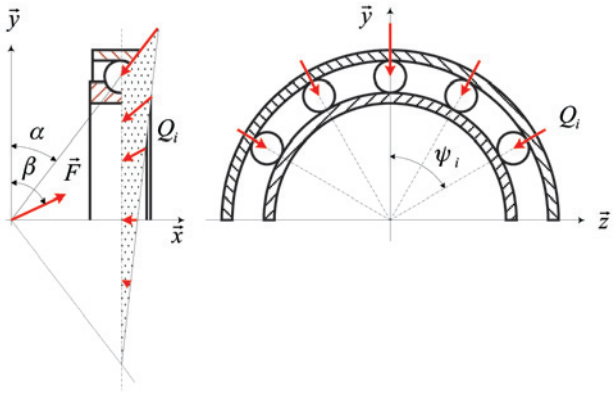

Figure 1. Loading forces and equilibrium conditions.

2.2. Loading Parameters

Suppose that the bearing is subjected to an external force $\vec{F}$, defined by

$$\vec{F} = F_a\vec{x} + F_r\vec{y} \tag{1}$$

where F_a and F_r are the axial and radial force components respectively, and

$$\tan\beta = \frac{F_a}{F_r} \tag{2}$$

where β is the angle between the loading force $\vec{F}$ and the radial direction (see Figure 1). The displacement of the inner ring (IR) relative to the outer ring (OR) will be expressed by

$$\vec{\delta} = \delta_a\vec{x} + \delta_r\vec{y} \tag{3}$$

where δ_a and δ_r are the axial and radial displacement components respectively.

The equilibrium condition (Figure 2) of the inner race, with N_b rolling elements, is

$$\vec{F} + \sum_{i=1}^{Nb} \vec{Q}_i = 0. \tag{4}$$

The load on any rolling element, at any angle ψ_i measured from the maximum load direction, is

$$Q_i = Q_{\max}\left[1 - \frac{1-\cos\psi_i}{2\varepsilon}\right]^{1.5} \qquad -\psi_m \le \psi_i \le \psi_m \tag{5-a}$$

$$Q_i = 0 \quad \text{elsewhere} \tag{5-b}$$

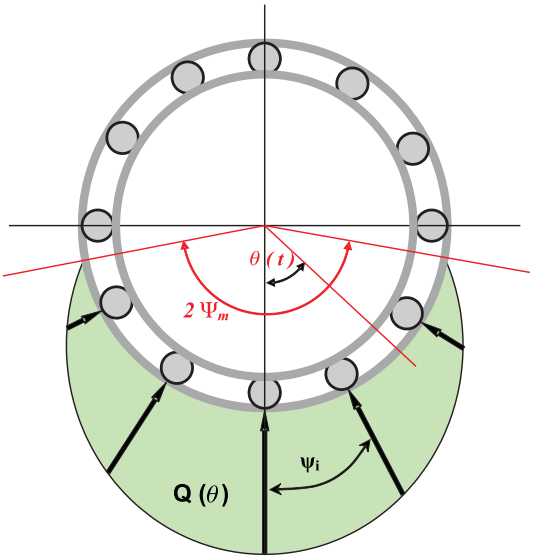

Figure 2. Load distribution under radial loading.

where ψ_m is the angular limit of the loading, as shown in Figure 2, $Q_{\max}$ is the maximum rolling element load and ε is the load distribution factor, defined by

$$\varepsilon = \frac{1}{2} \cdot \left[1 + \frac{\delta_a}{\delta_r} \cdot tg\alpha \right]. \tag{6}$$

Because of the various assumptions made in developing the model (small deformations, high number of balls, etc.), a comparative study was conducted using a finite element simulation of a 6206 deep groove ball bearing (20 mm bore, 47 mm outside diameter, 14 mm width, 34 mm pitch diameter, 0 degree nominal contact angle and 11 balls, each with a diameter of 7.5 mm) under a radial load of 1000 N and axial load of 200 N. Typical numerical results for the maximum rolling element load $Q_{\max}$ were computed and compared with the numerical results obtained from the finite element simulation, to help determine the effectiveness of the theory (see Table 1).

This comparison shows that the theory developed can be successfully used to predict static loads and stresses inside the bearing, with a discrepancy between the two methods of around 6%.

2.3. Defect Characteristics

Defects responsible for damage to the bearing can be either localized or distributed. Localized defects, generally occurring as a result of the fatigue process, include cracks, pits or spalls. Distributed defects, which are due to unavoidable manufacturing imperfections, include surface roughness, waviness, misaligned races and off-size rolling elements. Vibration responses caused by to localized defects are important in condition monitoring and system

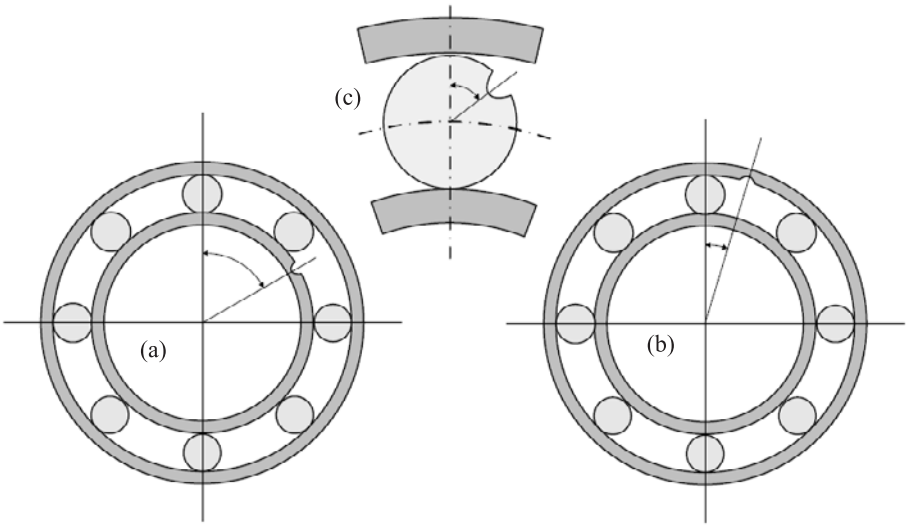

Figure 3. Different positions of localized defects affecting a ball bearing. (a) Defect on inner race. (b) Defect on outer race. (c) Defect on ball.

Table 1. Comparison between theoretical and numerical model values of static forces inside a type SKF 6206 bearing.

Maximum load (N)	$Q_{\max}$
Theoretical formula (12)	671
Finite element simulation	631
Relative error (%)	6 %

maintenance, while responses from distributed defects are used for quality inspection. Only localized defects are considered in this study. Such defects could affect the outer race, the inner race, the cage or the rolling elements. Irrespective of the defect component (whether it is located on the outer race, on the inner race, or on the ball), a hole with a regular (circular) geometry and characterized by a diameter d_{def} has been used to simulate the defect in this work (Figure 3).

If the outer race is not moving, any localized defect on its surface will have a constant angular position, usually corresponding to the direction of the external loading applied. However, if the inner race is rotating, any localized defect on its surface will be moving with the same velocity as the rest of the race. If the defect is localized on the rolling element surface, its motion will be a combination of cage and ball spin rotations.

2.4. Kinematics

Assuming a general configuration where both rings may rotate, the outer race is rotating at a constant speed ω_o and the inner race is rotating at a constant speed ω_i. The different frequencies generated by a bearing are (Taylor, 1994)

$$FTF = \frac{1}{2} \cdot \left[\omega_i \left(1 - \frac{B_d \cdot \cos\alpha}{P_d} \right) + \omega_o \left(1 + \frac{B_d \cdot \cos\alpha}{P_d} \right) \right] \quad (7\text{-a})$$

$$BPFO = \frac{Nb}{2} \cdot (\omega_i - \omega_o) \cdot \left(1 - \frac{B_d \cdot \cos\alpha}{P_d} \right) \quad (7\text{-b})$$

$$BPFI = \frac{N_b}{2} \cdot (\omega_i - \omega_o) \cdot \left(1 + \frac{B_d \cdot \cos\alpha}{Pd} \right) \quad (7\text{-c})$$

$$BSF = \frac{P_d}{2 \cdot B_d} (\omega_i - \omega_o) \cdot \left(1 - \frac{B_d^2 \cdot \cos^2\alpha}{P_d^2} \right) \quad (7\text{-d})$$

where *BPFO* is the ball pass frequency on an outer race defect, *BPFI* is the ball pass frequency on an inner race defect, *FTF* is the fundamental train frequency, *BSF* is the ball spin frequency, B_d is the ball diameter, P_d is the pitch diameter, N_b is the number of rolling elements and α is the contact angle. If the outer ring is fixed, it is sufficient to set ω_o equal to zero in equations (7) in order to determine the bearing frequencies (and similarly with ω_i if the inner ring is fixed).

3. SPECIFIC CHARACTERISTICS OF EXCITATION FORCES

The external excitation is the pulse generated whenever a defect on one of the races is struck by rolling elements, or when a defect on the rolling element strikes one of the races. The excitation action inside the bearing may be caused by the removal of large portions of hard surfaces as a result of subsurface fatigue. Any subsequent motion over the failed areas produces impacts which result in shock pulses. Such transient motions are commonly characterized by sudden occurrences and short durations.

3.1. Impact Force

Most rolling-element bearing applications involve the steady-state rotation of one or both races. The rotational speeds are usually moderate, so as to avoid ball centrifugal forces or significant gyroscopic motions and consequently these effects may be neglected.

The strength of the impact felt by the bearing components when the ball is traversing a defect area depends on the relative speeds and the external load applied. Therefore, we can easily imagine that the impact force should produce a static component, developed in equations (5), and a dynamic component arising from the impact of the ball against the edge of the defect area.

A shock is the transmission of kinetic energy to a system, occuring in a relatively short time. Assuming that the system is conservative, the conservation of mechanical energy between state 1 (before shock, see Figure 4) and state 2 (after shock) is

$$\left[\frac{1}{2} m V_1^2 + \frac{1}{2} I \omega_1^2 \right] + \left[mg \frac{B_d}{2} \right] = \left[\frac{1}{2} m V_2^2 + \frac{1}{2} I \omega_2^2 \right] + \left[mg \frac{B_d}{2} \cos\eta \right] \quad (8)$$

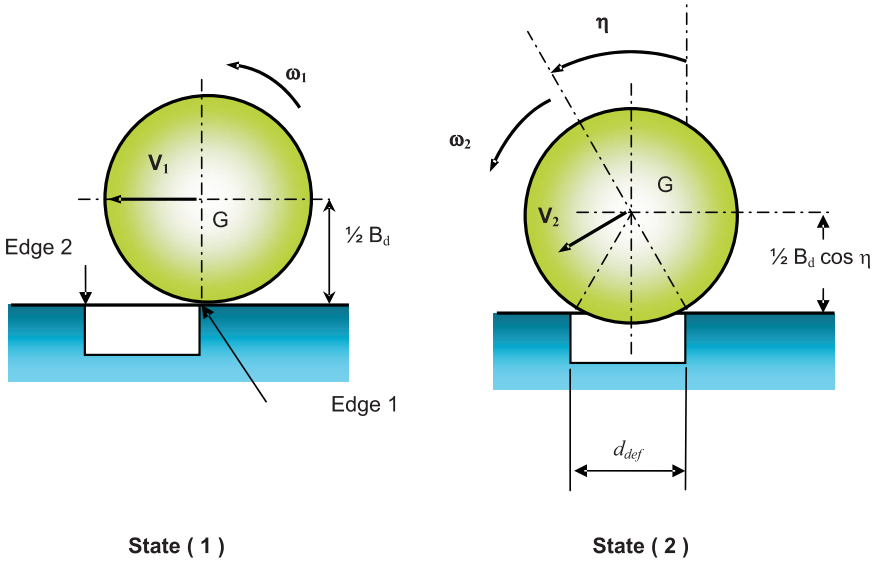

Figure 4. Kinematics of the ball motion around the edge of the defect area: State 1 is before shock, state 2 is after shock.

where $I = \frac{2}{5}m\left(\frac{B_d}{2}\right)^2$ is the ball mass moment of inertia and V and ω are, respectively, its linear and angular velocities, linked together by $V = (B_d/2)\,\omega$.

After rearranging the previous equation, we can conclude that

$$\Delta V^2 = V_2^2 - V_1^2 = \frac{10}{14} g B_d (1 - \cos\eta). \tag{9}$$

Assuming a small angle η, we can verify that

$$\sin\eta = \frac{\frac{d_{def}}{2}}{\frac{B_d}{2}} = \frac{d_{def}}{B_d} \approx \eta. \tag{10}$$

And therefore,

$$1 - \cos\eta \approx \frac{\eta^2}{2} = \frac{1}{2}\left(\frac{d_{def}}{B_d}\right)^2. \tag{11}$$

By substituting equation (11) into equation (9), the expression of ΔV^2 can be determined as

$$\Delta V^2 = V_2^2 - V_1^2 = \frac{10}{28} g B_d \left(\frac{d_{def}}{B_d}\right)^2 = Const \times \left(\frac{d_{def}}{B_d}\right)^2. \tag{12}$$

Experiments with bodies falling freely against a steel plate show that the impact force varies as the square of the shock velocity (Zhang et al, 2000). The expression of the dynamic (impacting) force, obtained from such experiments, is

$$F_D = K_{imp\_1} \Delta V^2 \tag{13}$$

where K_{imp_1} is a constant depending on the impacting material and the falling mass values. Excluding the mass (or static force F_S) from equation (13) gives us

$$F_D = K_{imp\_2} F_S \Delta V^2 \tag{14}$$

where K_{imp_2} is a constant depending only on the impacting material.

During the impact process, the total force striking the edge (2) is the sum of the static component, determined in equation (5), and the dynamic component, given in equation (14). Therefore, the total impacting force is

$$F_T = F_S + F_D \tag{15-a}$$

$$F_T = F_S \left(1 + K_{imp\_2} \Delta V^2\right). \tag{15-b}$$

Taking equation (12) into account, the expression of the total impacting force is

$$\begin{aligned} F_T &= F_S \left[1 + K_{imp\_2} \times \Delta V^2\right] = F_S \left[1 + K_{imp} \times \left(\frac{d_{def}}{B_d}\right)^2\right] \\ &= Q_{\max} \left(1 - \frac{1 - \cos \psi_i}{2\varepsilon}\right)^t \left[1 + K_{imp} \times \left(\frac{d_{def}}{B_d}\right)^2\right] \end{aligned} \tag{16}$$

where K_{imp} is the impacting coefficient, depending both on the impacting material and the bearing geometry.

Equation (16) suggests that the impact force is proportional to the square of the defect size width (expression of degree two). This formulation seems to be more accurate than the one proposed by Zhang (2000), in which the impact force is first degree with respect the defect size width and for which the error between theoretical and experimental values can be up to 15%.

3.2. Shock Pulses

The vibrations induced by impacts represent a transient phenomenon. Because of the rotation of the bearing, such impacts reappear periodically, depending on relative speeds, which produce repetitive shocks like a comb function. Therefore, the number of repeated impacts, and hence the frequency of the shock waves, are caused by the speed and the number of rolling bodies.

Let us examine the shock pulses produced by a single defect located on the race surface of a stationary outer ring of a bearing subjected to a fixed directional loading. All the rolling

bodies traverse the defect in the outer ring, and thus the frequency of hits depends on the speed of the bearing and the number of rolling bodies. The impacts repeat themselves with a constant amplitude and with equal periods (Figure 5a).

If the defect is affecting the rotating inner ring, the magnitude of the impacts will not be constant, but rather, will vary periodically, though they repeat themselves with equal periods. It is obvious that the impacts will be strong when the defect in the inner ring is in line with, and in the direction of the force acting on the bearing. The rolling element is rolling under it at just the same time. On the other hand, the impacts will be low when the defect is shifted from this position along the perimeter of the inner ring in any direction. Figure 5b illustrates the magnitude and rate of impacts. Wherever the defect is, the frequency of occurrence of maximum impact values is corresponding to the shaft speed. The modulation of the inner race fault signal at the shaft speed is due to both the periodically varying load on the fault and the periodically varying transfer function from a moving fault (Brie, 2000). A reverse effect appears when the load is rotating. In this case, the impact amplitudes on inner race are constants while they are modulated on the outer race.

If a defect is formed on a rolling body, it impacts against both the inner and outer races, i.e., there will be two impacts during one revolution of the rolling body (Thomas, 2002). These impacts will be strong when the defective ball is in the direction of the effective force as the defect impacts with one of the races. When the defective ball is located to one side of this position, the impact is weaker (Figure 5c). If two or more defects are found, pulse series are superimposed on each other.

4. VIBRATION MODEL OF BEARING ELEMENTS

Like all machines, bearings are built from many different parts, and calculating their exact dynamic behavior is very complicated, and sometimes not even possible. Therefore, a simple model is usually used to represent the whole bearing structure.

4.1. Model of the Rings

Whenever a defect, located at an angular position θ, is struck by the rolling element, inside a loaded area, the ring containing the defect is driven into a vibrating flexural motion. Such motion will theoretically occur in several different modes. However, in order to simplify the characterization of parameters, only the first vibration mode, which takes an elliptic shape, has been considered. The ellipse's long axis has been called the principal radial direction. It corresponds to the direction where the defect is applied, to the direction of the impulsive force and also to the direction of degrees of freedoms assumed by the model.

The inner and outer rings will each be represented by a mass-spring association corresponding to a single degree-of-freedom system. Internal damping has been neglected. The natural frequency for the flexural vibration mode number n is given (Nikolaou and Antoniadis, 2002) by

$$\omega_n = \frac{n\left[n^2-1\right]}{\sqrt{1+n^2}}\sqrt{\frac{EI}{\mu R^4}} \tag{17}$$

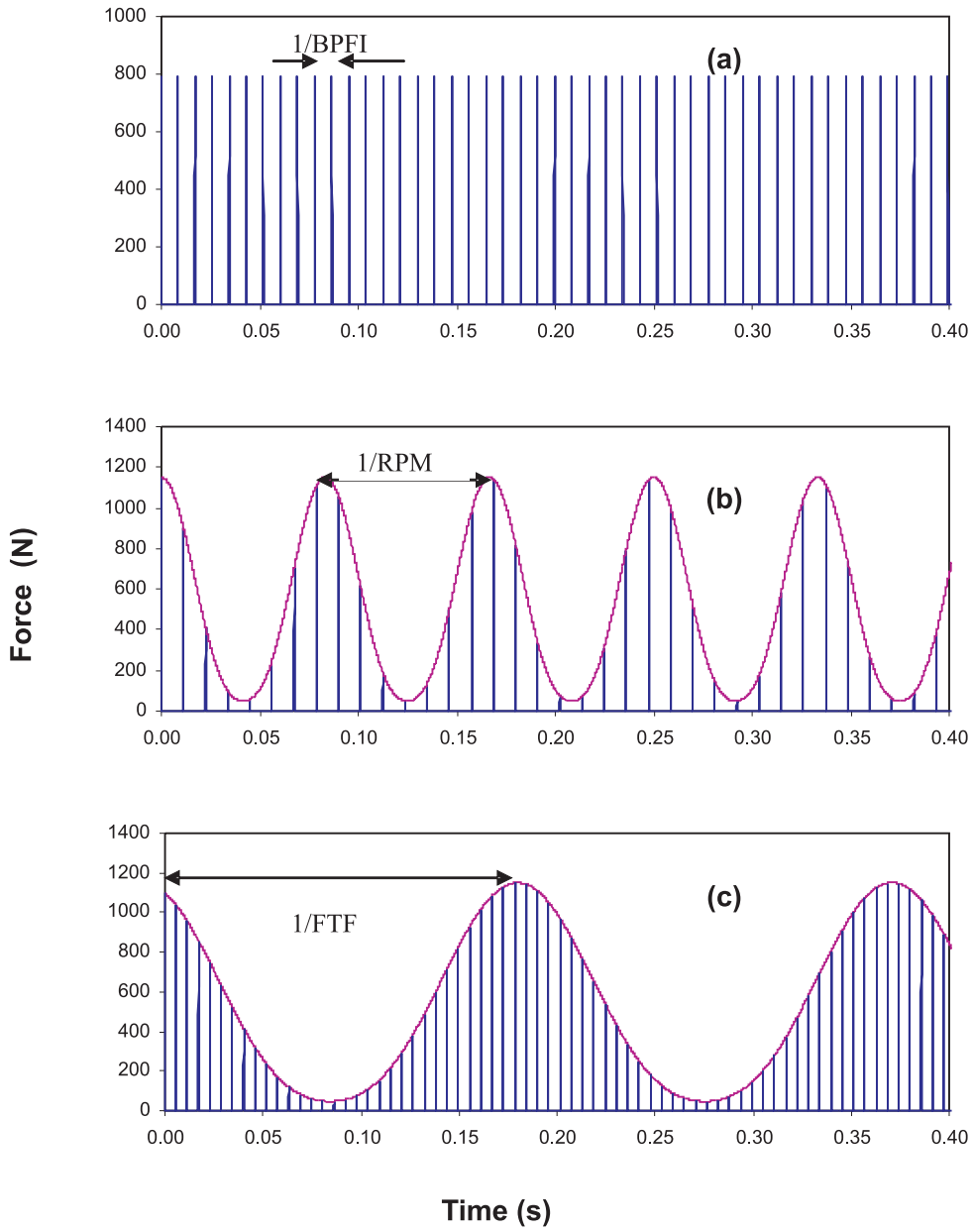

Figure 5. Shock pulses generated by a defect for a bearing (SKF 1210) with an inner ring rotating at 696 RPM, subjected to a rotating radial loading with a defect of 1 mm size located on: (a) Rotating inner race; (b) fixed outer race; (c) rolling element.

Table 2. Comparative study of flexural vibration frequencies by means of approximate formula and finite element simulation, applied to a type SKF 6206 bearing.

	Inner ring	Outer ring
Formula (17)	10 593 Hz	4 102 Hz
F.E. simulation	10 460 Hz	3 828 Hz
Relative error	1.25 %	6.68 %

where ω_n is the natural frequency of the ring [rad/s], E is the modulus of longitudinal elasticity [N/m^2], I is the moment of inertia of the cross-section of the ring [m^4], μ is the mass per unit length [kg/m], R is the radius of the neutral axis of the ring [m] and n is the order of the flexural vibration mode.

Because $n = 0$ and $n = 1$ correspond to rigid modes, flexural vibration modes start from $n = 2$. A comparative study with the results of the finite element simulation, applied to a bearing of type SKF 6206, shows that the previous formulation is quite accurate; see table 2.

Once the mass of the ring is known, its stiffness can be obtained as

$$K_{IR} = M_{IR} \cdot \omega_{IR}^2 \tag{18-a}$$

$$K_{OR} = M_{OR} \cdot \omega_{OR}^2 \tag{18-b}$$

where ω_{IR} and ω_{OR} are the natural frequencies of the first flexural modes ($n = 2$) of the two rings. A finite element simulation, applied to a type SKF 6206 bearing, shows that $K_{IR} = 2.48 \times 10^8$ N/m and $K_{OR} = 5.96 \times 10^7$ N/m. The inner ring is stiffer than the outer one.

4.2. Rolling Element Model

A finite element simulation, applied to a type SKF 6206 bearing, shows that the ball is the stiffest element in the bearing ($K_{ball} = 8.3 \times 10^9$ N/m). Consequently, these elements may be assumed to be infinitely rigid, allowing us to model it as a translating mass with a fair degree of confidence.

4.3. Model of the Lubrication Film Between Races and Balls

Until approximately 1960, the role of the lubricant between surfaces in rolling contact was not fully considered. Metal-to-metal contact was presumed to occur in all applications. The development of the elastohydrodynamic lubrication theory (EHD) showed that lubricant films with micrometer thickness occur in rolling contacts. Since surface finishes have similar thickness dimensions to the lubricant film, the significance of rolling-element bearing surface roughness in bearing performance became apparent. Therefore, the characterization of the lubrication regime depends on the thickness of the lubricant film.

Using the short-width-journal-bearing theory developed by Hamrock (1994), the dimensionless stiffness and damping coefficients of the fluid film can be expressed as

$$K = \frac{4}{W_r \lambda_k^2} \times \left[\frac{\varepsilon_0}{\left(1-\varepsilon_0^2\right)^2} \sin^2\phi_0 + \frac{3\pi\varepsilon_0^2}{4\left(1-\varepsilon_0^2\right)^{5/2}} \sin\phi_0 \cos\phi_0 + \frac{2\varepsilon_0\left(1+\varepsilon_0^2\right)}{\left(1-\varepsilon_0^2\right)^3} \cos^2\phi_0 \right] \quad (19)$$

$$C = \frac{4}{W_r \lambda_k^2} \times \left[\frac{\pi}{2\left(1-\varepsilon_0^2\right)^{3/2}} \sin^2\phi_0 + \frac{4\varepsilon_0}{\left(1-\varepsilon_0^2\right)^2} \sin\phi_0 \cos\phi_0 + \frac{\pi\left(1+2\varepsilon_0^2\right)}{2\left(1-\varepsilon_0^2\right)^{5/2}} \cos^2\phi_0 \right] \quad (20)$$

where

$$\frac{4}{W_r \lambda_k^2} = \frac{\left(1-\varepsilon_0^2\right)^2}{\varepsilon_0\left[16\varepsilon_0^2 + \pi^2\left(1-\varepsilon_0^2\right)\right]^{1/2}} \cos^2\phi_0 \quad (21)$$

$$\tan\phi_0 = \frac{\pi\left(1-\varepsilon_0^2\right)^{1/2}}{4\varepsilon_0} \quad (22)$$

$$\varepsilon_0 = 1 - \frac{h}{c}. \quad (23)$$

In these equations, ε_0 is the eccentricity ratio, c is the diametral clearance of the bearing, and h is the fluid film thickness. The diametral clearance c has been taken to be the mean of the min and the max values furnished by the bearing manufacturer. The film thickness h has been computed using the EHD theory.

4.4. General Model

If we consider the rotor, the bearing and the housing and supports, the model will rapidly become complex, with a large number of degrees of freedom.

In order to focus the study on the vibratory bearing response by retaining a simplified model, it has been found that applying a three DoF system for modeling the bearing system, as shown in Figure 6, was a good and sufficient assumption in order to focus the study on the vibratory bearing response in the principal radial direction or radial line Δm of maximum deformation. In this model, we consider only bearing behavior, and have modeled the bearing housings as infinitely rigid supports. We have not taken into account the contributions of the housing and supporting machine elements. Thus, this simplified model will need adjustments for computation of the amplitude of the vibratory response. See Figure 6 (in which M_{OR} is the mass of the outer ring [kg], M_{IR} is the mass of the inner ring [kg], M_B is the mass of the ball [kg], K_{OR} is the stiffness of the outer ring [N/m], K_{IR} is the stiffness of the inner ring [N/m], K_{OF} is the stiffness of the outer fluid film [N/m], K_{IF} is the stiffness of the inner fluid film [N/m], C_{OF} is the damping coefficient of the outer fluid film [N.s/m] and C_{IF} is the damping coefficient of the inner fluid film [N.s/m]) for a schematic of the model.

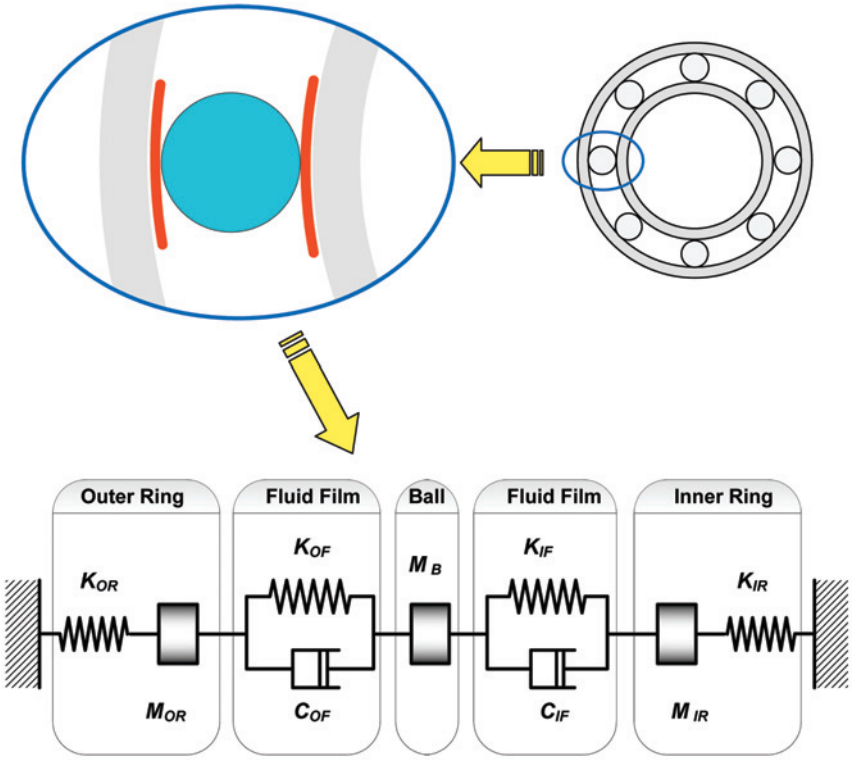

Figure 6. Bearing system model in the principal radial direction.

When the loading applied to the bearing is moderate, the bearing behavior can be assumed to be linear, and the mechanical system describing the bearing motion can be described by a linear inhomogeneous second order differential equation:

$$[M].\{\ddot{y}\} + [C].\{\dot{y}\} + [K].\{y\} = \{F\}. \tag{24}$$

Where the matrices [M], [K], and [C] are

$$[M] = \begin{bmatrix} M_{OR} & 0 & 0 \\ 0 & M_B & 0 \\ 0 & 0 & M_{IR} \end{bmatrix} \tag{25-a}$$

$$[K] = \begin{bmatrix} K_{OR}+K_{OF} & -K_{OF} & 0 \\ -K_{OF} & K_{OF}+K_{IF} & -K_{IF} \\ 0 & -K_{IF} & K_{IR}+K_{IF} \end{bmatrix} \tag{25-b}$$

$$[C] = \begin{bmatrix} C_{OF} & -C_{OF} & 0 \\ -C_{OF} & C_{OF} + C_{IF} & -C_{IF} \\ 0 & -C_{IF} & C_{IF} \end{bmatrix}. \tag{25-c}$$

The displacement vector $\{y\}$ along the radial direction and the force vector $\{F\}$ due to excitation shocks induced by rolling over surface defects are

$$\{y\} = \begin{Bmatrix} y_{OR} \\ y_B \\ y_{IR} \end{Bmatrix} \qquad \{F\} = \begin{Bmatrix} F_{OR} \\ F_B \\ F_{IR} \end{Bmatrix}. \tag{26-a}$$

All three components of vector {F} are calculated using the theoretical development of equation (16). If a single defect is affecting the bearing on its outer ring, its inner ring or one of its rolling elements, the forcing term of equation (26) will be

$$\{F\} = \begin{Bmatrix} F_{OR} = F_T \\ 0 \\ 0 \end{Bmatrix} \text{ or } \begin{Bmatrix} 0 \\ F_R = F_T \\ 0 \end{Bmatrix} \text{ or } \begin{Bmatrix} 0 \\ 0 \\ F_{IR} = F_T \end{Bmatrix}. \tag{26-b}$$

For the current work, SIMULINK was used to numerically solve equations (24), which represent the response of a bearing subjected to internal excitation from a localized defect. This response is subsequently processed numerically by a number of signal processing toolboxes to extract the needed information and curve plots.

5. GEOMETRIC RESPONSE CORRECTION

The model developed here was designed to generate a response corresponding to the radial line of maximum deformation Δ_m, whereas the real response measured by the sensor is given corresponding to a different radial line of measurement (Oy, see Figure 7).

In the case of a defect located on a rotating race, the angular position of the principal radial direction, which is the same as the model response, will also be rotating. This ring will be vibrating and turning at the same time, but the response given by a sensor is recorded in a fixed direction. Therefore, a correction coefficient must be added to the numerical response of the model to compensate for such phenomena and to force the numerical response to match the real response delivered by a fixed sensor.

The equation that describes the position of any point $M(\varphi)$ located on the rotating ellipse (which is assumed to be the first flexural vibration mode of the rotating ring in order to simplify the analysis) may be expressed as

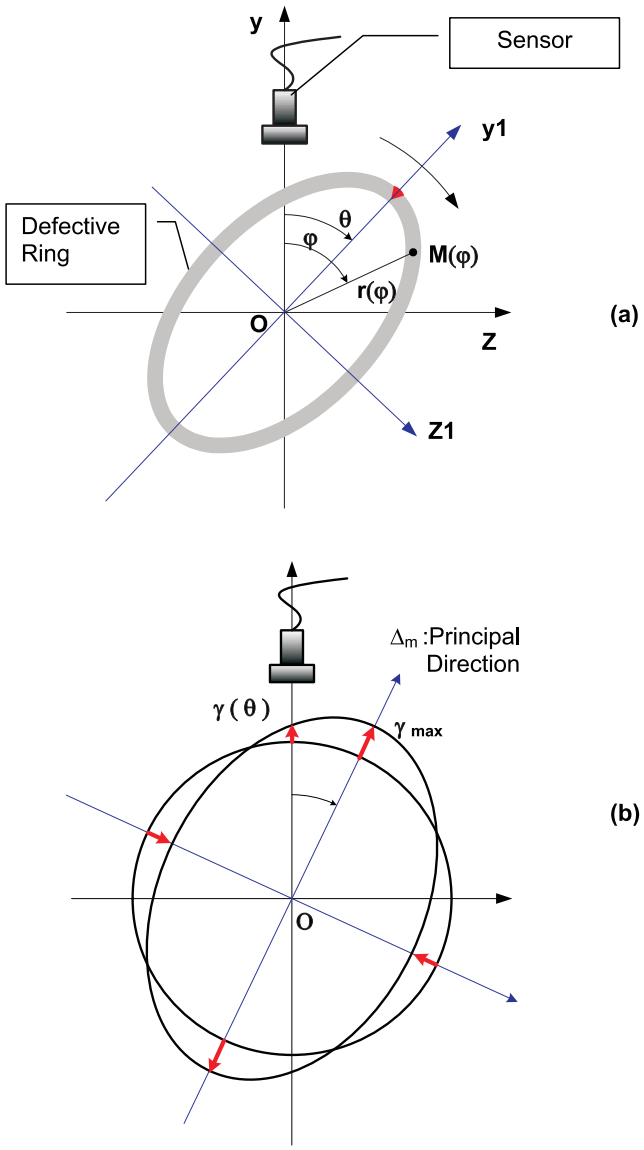

Figure 7. Deformation and measure directions for a defective vibrating ring. (a) Fixed and rotating ellipse, (b) First (elliptic) vibration mode of the ring.

$$r(\varphi) = \frac{ab}{\sqrt{a^2 \sin^2(\varphi - \theta) + b^2 \cos^2(\varphi - \theta)}} \tag{27}$$

where a and b are the long and short axes of the ellipse, locked to the referential $(O, y1, z1)$ coordinate system, which is directed at the angular position θ. A sensor placed at the vertical position ($\varphi = 0$) will be recording a displacement variation of the form

$$\gamma(\theta) = R - r(\varphi = 0) \tag{28-a}$$

$$\gamma(\theta) = R - \frac{ab}{\sqrt{a^2(\sin\theta)^2 + b^2(\cos\theta)^2}}. \tag{28-b}$$

Since the model developed here gives the vibration according to the maximal distortion direction, the response generated is $y_{\max} = a - R$. Knowing that the perimeter of the race is constant during the deformation, we can approximate to give

$$2\pi R \approx \pi(a + b). \tag{29}$$

After a few mathematical manipulations, we get the expression of the ring deformation measured by the sensor as

$$\gamma(\theta) = R - \left(\frac{\sin^2\theta}{\left[R - \gamma_{\max}\right]^2} + \frac{\cos^2\theta}{\left[R + \gamma_{\max}\right]^2} \right)^{-\frac{1}{2}}. \tag{30}$$

The angle θ is constant if the ring is immobile and variable if the ring is rotating.

6. EFFECTS OF RANDOM PERTURBATIONS

Due to increasing awareness of experimental results, it became standard to add a random element to the vibratory response, to allow for unconsidered disturbances (Brie, 2000). Among these disturbances, friction is a parameter that must be considered. Accurate experiments and laboratory observations generally show that bearings, irrespective of whether they are good or bad, or new or old, produce friction as the internal rolling elements turn against the inner and outer raceway. The notion of rolling without slip inside the bearing is purely hypothetical. The relative motion between the rolling elements and the races is comprised of a mixture of rolling and slip. When slip is present, stress waves are produced by the sudden internal stress redistribution of the materials caused by the changes in the internal structure. Such waves generate a random noise which can be measured by acoustic emission (AE), a technique that could be applied to monitor and control the health of the bearing. A theoretical model based on the deviation theory of a random function, has been developed for determining the parameters of AE accompanying the contact friction of solids (Barnov et al, 1997). According to this theory, the amplitude of AE is defined by the expression

$$Amplitude(AE) = K_{AE} V^{1/2} P^2 \tag{31}$$

where K_{AE} is a constant, V is the velocity of the surface sliding motion and P is the pressure on the surface of contact asperities.

Because random vibration and AE are both by-products of the same friction phenomenon, this random vibration (to be added to the main impulsive bearing response) could be expressed by a law of the form

$$\begin{aligned} &\textit{Amplitude (Random Vibration)} \\ &= K_N \cdot V^{1/2} \cdot \left(\frac{Q_{\max}}{CS_{ball-race}} \right)^2 \cdot f\left(\frac{d_{def}}{B_d} \right) \cdot Randn(t) \end{aligned} \tag{32}$$

where K_N is a constant, V is the relative slip speed between the ball and the race [m/s], $Q_{\max}$ is the maximum loading value given by equation (5) [N], $CS_{ball-race}$ is the ball/race elliptic contact surface [m^2], and $Randn(t)$ is a function of time that generates normally distributed random numbers.

The function f is a weighting function that depends on the ratio $\left(d_{def}/B_d\right)$. It may be expressed as a polynomial development of the 6^{th} degree, the coefficients of which are identified by an iterative process (after calibration from experimental measurements) to satisfy the condition

$$RMS\ (noise\ to\ add) = RMS\ (experimental\ data) - RMS\ (simulated\ data). \tag{33}$$

Equation (33) stipulates that the root mean square (*RMS*) value, contained in the experimental signal, is provided simultaneously by the noise and by the shock-induced vibration resulting from the simulation. The value of the constant K_N is obtained by assuming that the noisy signal should have a Kurtosis value of 3 in the absence of any localized defects (Thomas, 2002).

By adding the noise-producing term to the simulated impulsive response, which is caused by the localized defects, we obtain a general acceleration time response very similar to that given by a sensor during real experimental investigations. Figure 8 shows the effect on the initial signal of adding a random vibration. These time responses have been obtained by considering a defect of 0.55 mm size, located on the outer race (Figure 8a) or the inner race (Figure 8b) of a deep groove ball bearing type SKF 1210 (ETS test rig). The inner ring is rotating at 720 RPM and subjected to a rotating radial loading of 450 N caused by the unbalance and also to an axial loading of 1150 N.

Shock impulses generated by bearing faults excite the resonance frequencies of the bearing. Hence, a periodic sequence of excited vibrations is produced in the repetitive signal. These vibrations decay partially or completely until the onset of the next pulse.

7. AMPLITUDE CORRECTION

The shape of the measured time response is qualitatively very close to the one obtained numerically. However, the amplitudes of the experimental and numerical impulsive peaks are different, as the contribution of the housing and supporting machine elements has not been taken into account in the numerical model. Normalizing the experimentally obtained results and those from the numerical simulation to the same RMS amplitude for a particular size of localized defect would make the model predict the behavior of the damaged bearing inside its supporting environment.

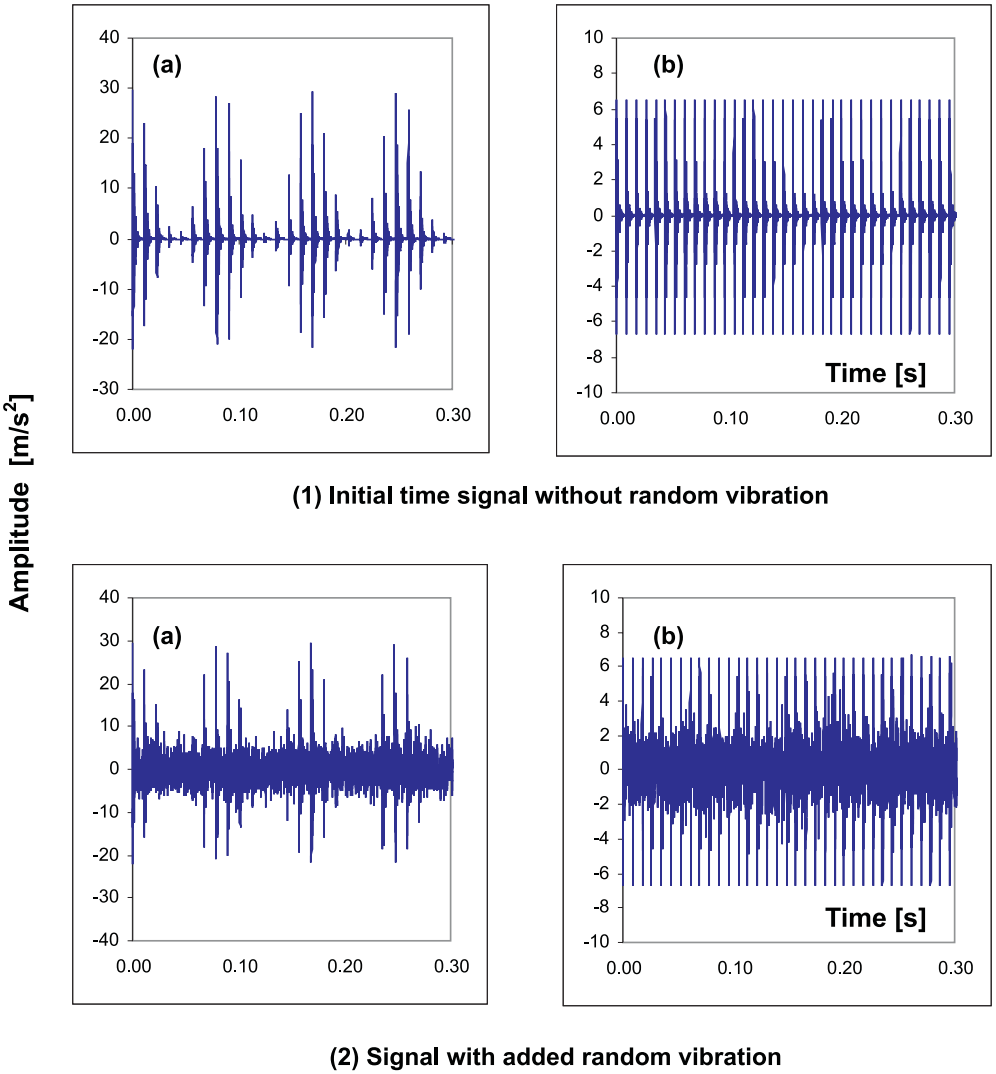

Figure 8. Time wave response (1) without and (2) with random vibrations (deep groove ball bearing type SKF 1210 with inner ring rotating at 720 RPM subjected to a rotating radial loading) with a defect of 0.55 mm size located on (a) outer race and (b) inner race.

8. RESULTS

To gain a detailed insight into the dynamic behavior of rotating bearings when they are affected by localized defects, a user-friendly software tool called BEAT® (BEAring Toolbox), which includes all the theoretical elements developed in this article, has been produced within the MATLAB environment. Because the radial forces can be applied to the bearing in either a fixed direction (e.g., hydraulic actuator) or a rotating direction (e.g., unbalance), an extra module has been added to BEAT to allow it to take both cases of radial loading

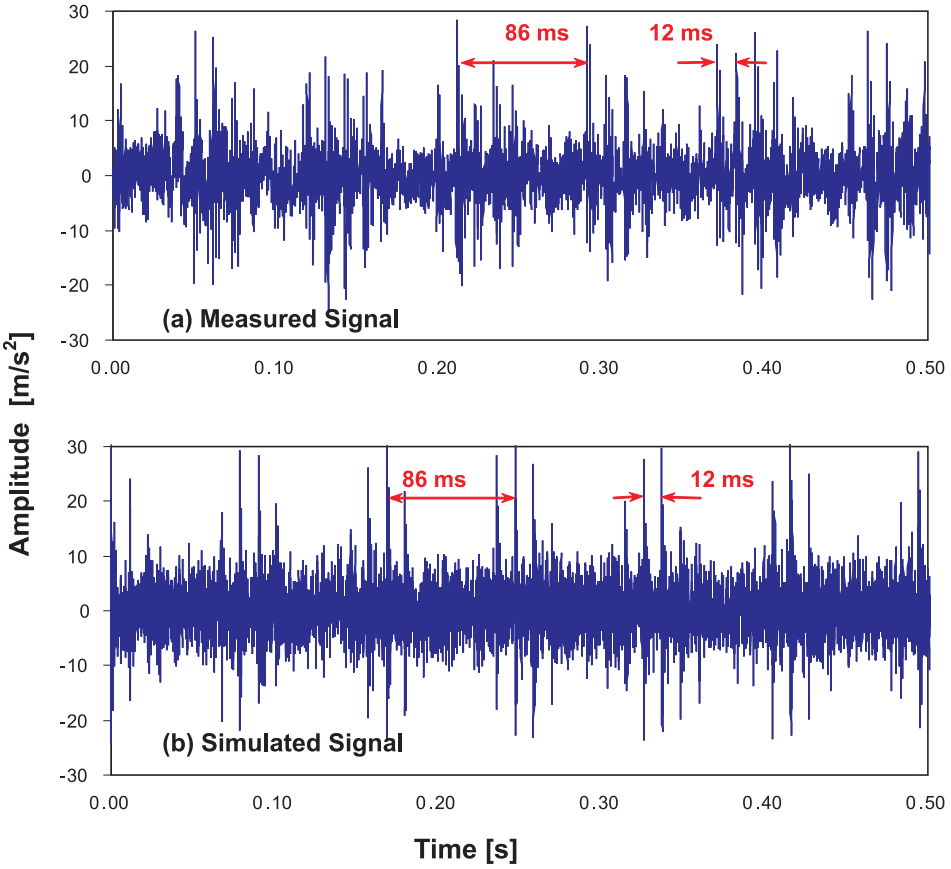

Figure 9. Time domain signal for a damaged self-aligning bearing (type SKF 1210 ETK9) with 550 μm defect located on the outer race and rotation frequency of 11.6 Hz.

into account. The experimental results used for comparison in the case of a fixed direction radial force were directly downloaded from the "Bearing Data Center (B.D.C.)" Website of Case Western Reserve University, Cleveland, Ohio, USA (2006). Results for a rotating direction radial force were measured on a home made test rig, originally located at the vibration & acoustic laboratory of the Ecole de Technologie Supérieure (E.T.S.), Montreal, Quebec, Canada.

Qualitative and quantitative comparisons of several results (in the time and frequency domains) obtained from experimental and simulation signals clearly shows that the model developed provides realistic results which are very similar to those given by a sensor during experimental measurements.

8.1. Time Analysis

Figure 9 compares the time signals produced in acceleration by the numerical model and experimental measurements for a bearing with a damage size equal to 550 μm on the outer

Table 3. Scalar indicators specific to ball bearing vibration detection.

Peak	$a_{PEAK} = \max \lvert a_k \rvert_{1 \le k \le N}$	(36-a)
Average	$\bar{a} = \frac{1}{N} \sum_{k=1}^{N} a_k$	(36-b)
Root mean square	$a_{RMS} = \sqrt{\frac{1}{N} \sum_{k=1}^{N} a_k^2}$	(36-c)
Crest factor	$CF = \frac{a_{PEAK}}{a_{RMS}}$	(36-d)
Kurtosis	$KU = \frac{\frac{1}{N} \sum_{k=1}^{N} (a_k - \bar{a})^4}{a_{RMS}^4}$	(36-e)
Shape factor	$SF = \frac{a_{RMS}}{\frac{1}{N} \sum_{k=1}^{N} \lvert a_k \rvert}$	(36-f)
Impulse factor	$IF = \frac{a_{PEAK}}{\frac{1}{N} \sum_{k=1}^{N} \lvert a_k \rvert}$	(36-g)

Table 4. Comparison between time domain indicators collected from BDC test rig and simulated on BEAT.

	Experimental results (one measurement)	Numerical results (BEAT) (100 simulations)	Error (%)
PEAK	10.1	10.26	1.6
RMS	2.1	2.09	0.5
C.F.	4.9	4.91	0.2
KU	3.9	3.66	6.2
I.F.	6.4	6.27	2
S.F.	1.3	1.28	1.6

race and excited by an unbalance rotating at 695 rpm. The time it takes for the inner race to make one revolution is 86.4 ms. The computed BPFO is 86 Hz, and the time for one outer race ball pass is 11.6 ms. The two signals in Figure 9 show notable similarities. About 0.5 s are displayed for both experimental and numerical results. The information in the two figures is proof of the ability of the BEAT software to predict the behavior of a bearing affected by a localized defect in the time domain.

A comparison between the experimental value of scalar indicators (as defined in Table 3) extracted from time signals (Case Western Reserve University, 2006) and those obtained from 100 numerical simulations is presented in Table 4. The bearing considered is of type

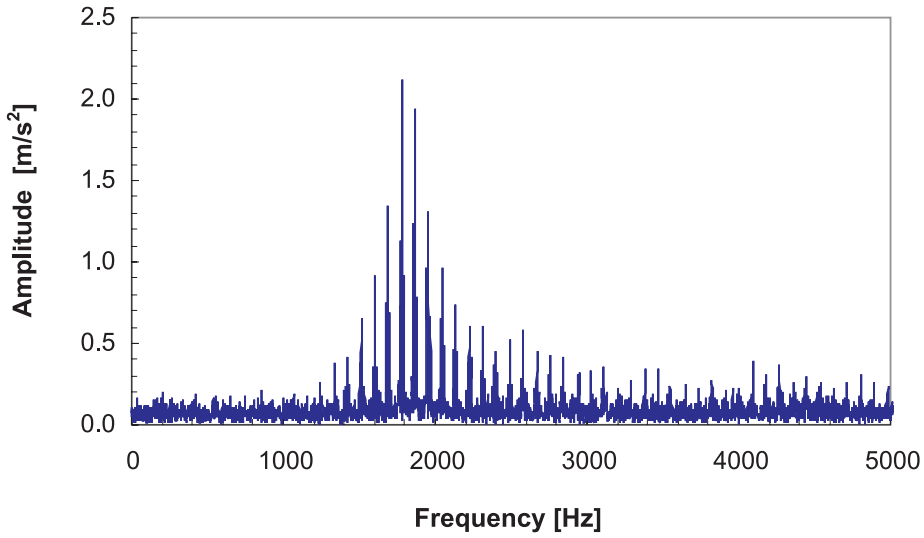

Figure 10. Spectrum of a damaged deep groove ball bearing (type SKF 1210 ETK9) with 1 mm defect located on the outer race and rotation frequency of 11.6 Hz.

SKF 6205, and has nine balls and a pitch-diameter-to-ball-diameter ratio of 4.9. The faults are located on the inner race. The maximum damage size is 0.72 mm, the rotor speed is 1750 rpm, and the radial force applied to the bearing is maintained in a fixed direction.

Because of the perturbation term added to the impulsive response, the average values of these parameters computed for 100 simulations and compared to the experimental trial show a very good agreement, with a maximum error of 6.2 %.

8.2. Frequency Analysis

A defect could be quantified by measuring the peak amplitudes at the characteristic defect frequencies (FTF, BPFO, BPFI or BSF) or their harmonics. The evolution of a fault in a rolling element bearing will not only cause an increase in the amplitude of vibration at the characteristic defect frequencies, but will also generate harmonics of these frequencies and modulation components. The key for diagnosing problems using spectrum analysis lies in looking at how many harmonics are present in the signal, and in evaluating their modulating frequencies.

In fact at the second stage of degradation as defined by Berry (1991), defects in the rolling element bearing generate a signal that modulates the natural frequencies with bearing frequencies. Figure 10 shows, by way of example, the FFT of the simulated time response from Figure 9b. It can be observed a signal with large amplitudes in the high frequency domain at the resonance frequency of the bearing (close to 2000 Hz) and modulated by a lot of harmonics.

This result has been obtained considering the bearing discretized as a three DoF system and with other simplifications; notably without considering the rotor, the housing and

the supports. Consequently, the natural frequencies cannot be compared with experimental results that take into account all the resonant frequencies of the bearing and its surroundings. Instead of the natural frequencies, the defect diagnosis is more concerned with the modulation frequencies.

Demodulation or enveloping-based methods offer the strongest reliable diagnostic potential of present methods. The general assumption with the enveloping approach is that a measured signal contains a low-frequency phenomenon that acts as the modulator to a high-frequency carrier signal. In bearing failure analysis, the low-frequency phenomenon is the impact caused by a defect of a bearing; the high-frequency carrier is a combination of the natural frequencies of the associated rolling element or of the machine it forms part of. The goal of enveloping is to replace the oscillation caused by each impact with a single pulse over the entire duration of the impact response. Several demodulation methods have been used to identify faults in rolling element bearings. The most widely used and well-established of these is based on the Hilbert transform. This method was used to obtain Figure 11, which compares the experimental and numerical envelopes produced by a defect on the outer race of the ETS test rig.

As expected, both results show the appearance of harmonics of BPFO modulated by the fundamental frequency. The appearance of these frequencies is a typical key for diagnosing a damaged bearing at its third level of severity. It can be seen that the measured and numerical envelope spectra are similar, but that the effects of the harmonics and sidebands are amplified in the simulation.

Figure 12 shows another envelope spectra obtained from the experimental data that were furnished by the Website of Case Western Reserve University (2006). This case uses a SKF 6205 bearing with nine balls and a pitch-diameter-to-ball-diameter ratio of 4.9. The depth of the defects (0.72 mm) was chosen such that the balls span the gap without bottoming. The rotor speed is 1750 rpm. The radial force applied to the bearing is maintained in a fixed direction. The numerical results are compared with the experimental data for a defect located on the inner race. It can easily be seen from Figure 12 that many qualitative and quantitative similarities are observed in the envelope spectra (harmonics and side bands of the bearing defect frequency).

Even if the measured signal is richer in frequency due to the effect of the motor and surrounding supports which were not considered in the numerical simulation, the harmonics produced by the defect are pretty well predicted. As expected, both results show the appearance of harmonics of BPFI modulated by the fundamental frequency. The appearance of these frequencies is a typical key for diagnosing a damaged bearing at the third level of severity.

9. CONCLUSIONS

A theoretical model of a ball bearing is developed to obtain the vibration response due to localized surface defects. For purposes of simplification, the bearing is modeled as a 3 DoF system. The system impulse response is obtained in terms of the rotation of the bearing, the distribution of the load in the bearing, the elasticity of the bearing structure, the elasto-

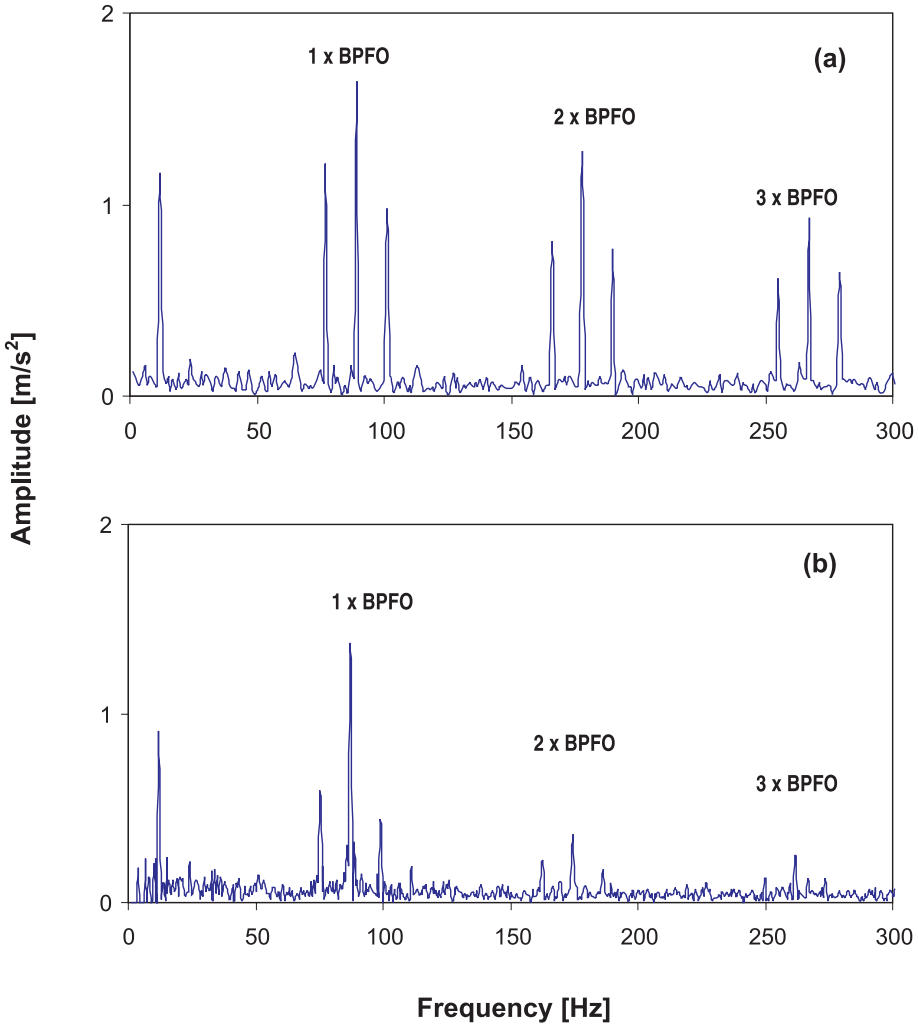

Figure 11. Comparison of envelope spectra for a damaged ball bearing (type SKF 1210) with 1270 μm defect on outer race and rotation frequency of 11.6 Hz. (a) Simulated results produced with BEAT. (b) Measured results from ETS test rig.

hydro-dynamic oil film characteristics and the transfer function between the bearing and the transducer.

The proposed model includes several new considerations. The total impacting force has been modified to take into account two parts: The static force present in other published models and an additional part accounting for the shock produced by the defect. In order to compare numerical results with experimental measurements coming from a sensor, a geometric correction of the response has also been added to take into account the fact that the damaged ring will be vibrating and turning at the same time, whereas the results given by a sensor are recorded in a fixed direction.

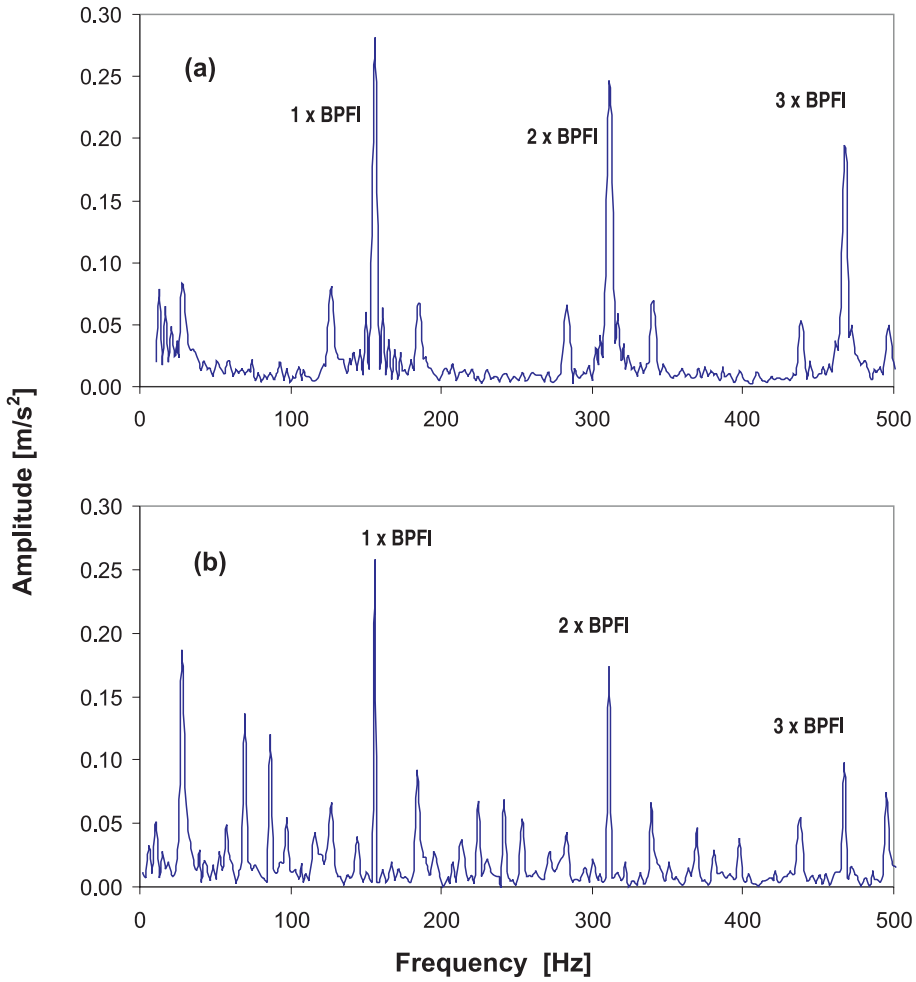

Figure 12. Comparison of envelope spectra for a damaged ball bearing (type SKF 6205-2RS JEM) with 0.72 mm defect on inner race; speed of rotation is 1750 rpm and power applied is 2 hp. (a) Simulated results produced with BEAT. (b) Measured results from BDC test rig.

Finally, by adding a noisy response resulting from sliding friction between the moving parts and other disturbances to the impulsive response due to localized defects, the proposed model is able to provide results similar to those produced by a sensor during experimental measurements.

However, the proposed method has the disadvantage that it requires calibration by experimental measurements in order to take into account unconsidered disturbances and the limits of the model. On the other hand, this calibration has the advantage that the predicted results take account of factors specific to the bearing being considered, increasing confidence in the prediction.

A friendly user software toolbox called BEAT®, which includes all of these elements, has been produced within the MATLAB environment.

The results produced by the numerical model have been compared in both the time and frequency domains with signatures obtained from experimental data for bearings with various sizes of surface defect. The BEAT® software consistently generates an output close to the experimental values obtained from real-world testing. From all the comparisons between simulated and experimental results (more than 100 numerical simulations), it was concluded that BEAT® is able to predict the dynamic behavior of the damaged bearing with a degree of confidence greater than 85 %.

Acknowledgements. The agreement of the "Bearing Data Center" (Case Western Reserve University, Cleveland, Ohio, USA) to use their Seeded Fault Test Data is gratefully acknowledged. The authors thank the Natural Science and Engineering Research Council of Canada (NSERC) program for its financial support.

REFERENCES

Aleyaasin, M., Ebrahimi, M., and Whalley R., 2000, "Vibration analysis of distributed-lumped rotor systems," *Computer Methods in Applied Mechanics and Engineering* **189(2)**, 545–558.

Barnov, V. M., Kudryavstev, E. M., and Sarychev, G. A., 1997, "Modelling of the parameters of acoustic emission under sliding friction of solids," *Journal of Wear* **202(2)**, 125–133.

Berry, J., 1991, "How to track rolling bearing health with vibration signature analysis," *Journal of Sound and Vibration* **25(11)**, 24–35.

Brie, D., 2000, "Modelling of the spalled rolling element bearing vibration signal: An overview and some new results," *Journal of Mechanical Systems and Signal Processing* **14(3)**, 353–369.

Case Western Reserve University, Bearing Data Center, 2006, http://www.eecs.cwru.edu/laboratory/bearing/download.html

El Saeidy, F. M. A., 1998, "Finite element modeling of a rotor shaft rolling bearings system with consideration of bearing nonlinearities," *Journal of Vibration and Control* **4(5)**, 541–602.

Fang, H. and Yang, B., 1998, "Modeling, synthesis and dynamic analysis of complex flexible rotor systems," *Journal of Sound and Vibration* **211(4)**, 571–592.

Hamrock, B. J., 1994, *Fundamentals of Fluid Film Lubrication,* McGraw-Hill, Singapore.

Lim, T. C. and Singh, R., 1990, "Vibration transmission through rolling element bearings, part 1: Bearing stiffness formulation," *Journal of Sound and Vibration* **139(2)**, 179–199.

McFadden, P. D. and Smith, J. D., 1984, "Model for the vibration produced by a single point defect in a rolling element bearing," *Journal of Sound and Vibration* **96(1)**, 69–82.

Nikolaou, N. G. and Antoniadis, I. A., 2002, "Demodulation of vibration signals generated by defects in rolling element bearings using complex shifted morlet wavelets," *Mechanical Systems and Signal Processing* **16(4)**, 677–694.

Shamine, D. M., Hong, S. W., and Shin, Y. C., 2000, "An in-situ modal-based method for structural dynamic joint parameter identification," *IMechE Journal of Mechanical Engineering Science* **C214(5)**, 641–653.

Spiewak, S. A. and Nickel, T., 2001, "Vibration based preload estimation in machine tool spindles," *International Journal of Machine Tools and Manufacture* **41(4)**, 567–588.

Su, Y. T., Lin, M. H., and Lee, M. S., 1993, "The effects of surface irregularities on roller bearing vibrations," *Journal of Sound and Vibration* **165(3)**, 455–466.

Sunnersjo, C. S., 1985, "Rolling bearing vibrations: The effects of geometrical imperfections and wear," *Journal of Sound and Vibration* **98(4)**, 455–474.

Tandon, N. and Choudhury, A., 1997, "An analytical model for the prediction of the vibration response of rolling element bearings due to a localized defect," *Journal of Sound and Vibration* **205(3)**, 275–292.

Taylor, J. I., 1994, *The vibration analysis handbook*, Vibration Consultants, Tampa, FL.

Thomas, M., 2002, *Fiabilité, maintenance prédictive et vibrations de machines,* (in French) ETS editions, Montréal, Canada.

Zhang, C., Qiu, J., Kurfess, T. R., Danyluk, S., and Liang, S. Y., 2000, "Impact dynamics modeling of bearing vibration for defect size estimation," *International Journal of COMADEM* **3(3)**, 37–42.